Colloids and Surfaces B: Biointerfaces 141 (2016) 499–506

Contents lists available at ScienceDirect

Colloids and Surfaces B: Biointerfaces

journal homepage: www.elsevier.com/locate/colsurfb

Hyaluronan/chitosan nanofilms assembled layer-by-layer and their antibacterial effect: A study using *Staphylococcus aureus* and *Pseudomonas aeruginosa*

J. Hernandez-Montelongo[a,*], E.G. Lucchesi[b], I. Gonzalez[c], W.A.A. Macedo[c], V.F. Nascimento[d], A.M. Moraes[d], M.M. Beppu[d], M.A. Cotta[a]

[a] Departamento de Física Aplicada, Instituto de Física Gleb Wataghin, Universidade Estadual de Campinas, Campinas, 13083-859 São Paulo, Brazil
[b] Itibanyl Produtos Especiais LTDA, Jarinu, 13240-000 São Paulo, Brazil
[c] Centro de Desenvolvimento da Tecnologia Nuclear, 31270-901 Belo Horizonte, Mina Gerais, Brazil
[d] Faculdade de Engenharia Química, Universidade Estadual de Campinas, Campinas, 13083-852 São Paulo, Brazil

ARTICLE INFO

Article history:
Received 14 November 2015
Received in revised form 1 February 2016
Accepted 10 February 2016
Available online 12 February 2016

Keywords:
Hyaluronan/chitosan nanofilms
Biopolymers
Layer-by-layer
Staphylococcus aureus
Pseudomonas aeruginosa

ABSTRACT

In the last few years, chitosan-based coatings have been proposed as antibacterial surfaces for biomedical devices in order to prevent nosocomial infections. In that sense, this work reports the optimized synthesis of hyaluronan/chitosan (HA/CHI) nanofilms assembled layer-by-layer in order to maximize the antibacterial effect for two important human pathogenic bacteria, *Staphylococcus aureus* and *Pseudomonas aeruginosa*. In this assembly, HA forms a soft, highly hydrated, and nontoxic film, whereas CHI shows the antimicrobial characteristics. Our HA/CHI nanofilm synthesis optimization was based on changing pH values of the biopolymer stem-solutions and the consequent variation of their ionization degree. Furthermore, the surface density of primary amino groups, which are related to the antibacterial effect, was also enhanced by increasing the number of HA/CHI bilayers. The antibacterial effect of HA/CHI nanofilms was evaluated by the spread plate counting method for both bacteria. These results were correlated with the morphology of nanofilms (characterized using SEM and AFM), as well as with their chemical properties studied by UV–vis, Kelvin Probe Force microscopy and XPS spectroscopy.

1. Introduction

Nosocomial infections are those developed in patients during their stay in a hospital. Such infections occur in 5–10% of all hospitalizations in Europe and North America; this percentage, however, reaches more than 40% in parts of Asia, Latin America, and sub-Saharan Africa [1]. Nosocomial infections are generally caused by opportunistic microorganisms, among which the most prevalent Gram-positive bacteria are different strains of *Staphylococcus aureus* and *Enterococcus* genus [2]. The most predominant Gram-negative bacteria are *Pseudomonas aeruginosa*, *Stenotrophomonas maltophilia*, *Enterobacteriaceae* family and *Acinetobacter* genus [2]. Both *S. aureus* and *P. aeruginosa* have become the most important cause of nosocomial infections in recent years. Their pathogenicity is mainly due to the ability to form biofilms on biomedical devices and prosthesis [3,4]. In the latter case, thin surface coatings for both attachment reduction and larger bacterial killing rates are mandatory [5].

Due to its antibacterial properties, biocompatibility and biodegradability, chitosan (CHI) is an excellent alternative to coat biomedical devices to prevent nosocomial infections [6]. It has been successfully used against both gram-negative and gram-positive bacteria [7]. Two mechanisms have been proposed as the main cause of antibacterial action by CHI. One is that the polycationic nature of chitosan interferes with bacterial metabolism by electrostatic interactions at the negatively charged cell surface of bacteria, and the other one is blocking of transcription of RNA from DNA by adsorption of penetrated CHI to DNA molecules [7].

In the last years, different chitosan-based nanofilms assembled layer-by-layer (LbL) have been used as antibacterial coatings, either as a single, pristine film [5,8–10] or enhanced with antimicrobial species, such as peptides [11,12] or silver nanoparticles [13]. The simplicity, versatility, and nanoscale control that LbL assembly provides make it one of the most widely used technologies for coatings applied in biomedicine and other fields [14]. LbL is a simple bottom-up technique, which consists of alternating physisorption

* Corresponding author.
E-mail address: jacobo@ifi.unicamp.br (J. Hernandez-Montelongo).

http://dx.doi.org/10.1016/j.colsurfb.2016.02.028
0927-7765/

of oppositely charged polyelectrolytes. For biomedical applications, the hyaluronan (HA, a polyanion) can be used in combination with CHI (a polycation) for the synthesis of antibacterial coatings by the LbL technique: HA forms a soft, highly hydrated, and nontoxic film, whereas CHI has the antimicrobial characteristics [10].

Previous works have assembled HA and CHI by LbL for biomedical applications. Richert et al. [15] studied the influence of salt concentration, Chua et al. [11] coupled HA/CHI films with surface-immobilized cell-adhesive arginine-glycine-aspartic acid (RGD) peptide, and Cui et al. [16] quaternized CHI with glycidyltrimethylammonium chloride (GTMAC) to build up microcapsules. Richert et al. [15] obtained an 80% reduction of *E. coli* adhesion after 30 min of cell culture. In the case of Chua et al. [11] and Cui et al. [16], for a cell culture of 4 h, they reported an 80% decreasing of *S. aureus* and ~100% reduction of *Escherichia coli*, respectively. In our work, we focus on the synthesis and optimization of the antibacterial effect up to 8 h of culture of HA/CHI nanofilms assembled by LbL. Optimization was performed by varying specific pH values of polyelectrolyte solutions, which control the ionization degree of each biopolymer. Moreover, due to the exponential growth trend exhibited by the thickness of our nanofilms, the surface density of amino groups, which are associated with the antibacterial effect, was also enhanced by increasing the number of HA/CHI bilayers. Surface properties of HA/CHI assemblies were monitored in each alternating deposition; the final physicochemical properties of our samples were correlated with their antibacterial effect against the human pathogenic microorganisms *S. aureus* and *P. aeruginosa*.

2. Materials and methods

2.1. Materials

Polyethylenimine (PEI, 50 wt.% solution in water, $M_W \approx 7.5 \times 10^5$ g/mol), hyaluronic acid sodium salt (HA, from *Streptococcus equi* sp, $M_W \approx 1.58 \times 10^6$ g/mol), chitosan (CHI, 75–85% deacetylated, low $M_W \approx 5 \times 10^4$ g/mol), methylene blue (MB, $M_W \approx 373.90$ g/mol), and rose Bengal (RB, $M_W \approx 1017.64$ g/mol) were purchased from Sigma-Aldrich, USA. Sodium hydroxide (NaOH), sodium chloride (NaCl), and hydrochloric acid (HCl) were purchased from Synth Brazil. All chemicals were used without further purification, and solutions were prepared using Milli-Q water with resistivity of 18.2 MΩcm (pH ~7.6, otherwise mentioned). Silicon (Si) wafers with <100> orientation were used as substrates and purchased from University Wafer, USA.

2.2. Polyelectrolyte solutions

Polyelectrolyte solutions were prepared by dissolving the respective polymer in Milli-Q water at concentrations of 1% (w/v). PEI was dissolved in a 0.5 M NaCl solution and its pH was adjusted to 4. HA and CHI were dissolved in a 0.17 M NaCl solution and their pH was adjusted at three different values: 4.5, 3 and 2. The CHI solution was also prepared with 100 mM glacial acetic acid. All solutions were stirred overnight and their pH values were adjusted with a 0.1 M HCl and/or NaOH solution.

2.3. Substrate preparation

Si substrates were cleaned by ultra-sonication for a period of 15 min each in acetone, isopropanol and distilled water, respectively. Afterwards, Si wafers were dried under N_2 flow and subsequently treated with O_2 plasma at 100 mTorr for 15 min (720 V DC, 25 mA DC, 18 W; Harrick Plasma Cleaner, PDC-32G). A single PEI pre-layer was deposited onto the substrates using an automatic dipping procedure (LbL Nanostructure Pro, ECSIA NanoScience, Brazil) with constant stirring under room conditions. Substrates were immersed in the PEI solution for 15 min, followed by three consecutive Milli-Q water rinse steps of 2, 1 and 1 min, respectively. The pH of water rinse was previously adjusted at 4.

2.4. Polyelectrolyte multilayer assembly

Substrates were alternately immersed in HA and CHI solutions for 15 min; each layer was followed by three consecutive Milli-Q water rinse steps of 2, 1 and 1 min, respectively. HA/CHI nanofilms were assembled on substrates by LbL using the previous mentioned automatic dipping equipment under ambient conditions and constant stirring. The pH of the polyelectrolytes and rinsing water was adjusted according to the respective assembling conditions. The LbL procedure was repeated for three or nine cycles in each case, with the CHI coating on the top.

2.5. Physicochemical characterization

HA/CHI assemblies were monitored by measuring their respective water contact angle in each alternating deposition. A contact angle goniometer Easy DropDSA-150 goniometer Krüss (Germany) was used in the static sessile drop mode. The morphologies of the samples were observed by field-emission scanning electron microscopy (FESEM; model F50, FEI Inspect) operated with a tilt of 45° at 2 keV. Prior to examination, samples were coated with sputtered gold to prevent electrical charging.

The topography of the nanofilms was acquired by atomic force microscopy (AFM) using a Keysight equipment Model5500 (Keysight Technologies, Chandler, AZ, USA). Images were acquired in tapping mode in air using conical Si tips with a typical tip radius of 10 nm and tip length of ~20 μm (MPP-21120-10, Veeco, NY, USA). The spring constant and resonance frequency were typically 3 Nm^{-1} and 75–95 kHz, respectively. To evaluate the roughness of the surface, the root-mean-squared roughness (R_{RMS}) was determined over 5×5 μm^2 areas for each sample.

Surface potential was assessed by Kelvin Probe Force Microscopy (KPFM) measurements, acquired simultaneously with topography in tapping mode under N_2 flow using Pt-coated Si tips (SCM-PIT/Pt, Bruker, CA, USA). The spring constant and resonance frequency of the tips were typically 3 Nm^{-1} and 75–95 kHz, respectively. All AFM and KPFM images, thickness measurement, roughness calculations and surface potential analysis were processed using freely available software (Gwyddion V. 2.37).

To evaluate the presence of free carboxylic and amino groups in PEMs, samples were immersed in MB and RB solutions, followed by three consecutive Milli-Q water rinse steps of 2, 1 and 1 min, respectively. Subsequently, stains from both sides of the slides (6 cm^2 of total area) were removed for UV–vis spectroscopy measurements on absorbance mode. Samples with MB were immersed in a solution of glacial acetic acid at 5% (v/v), and samples with RB were immersed in a solution of 1 M NaOH. MB and RB absorbance values were detected at 663 nm and 545 nm, respectively, by using a UV–vis VarianCary 1 G (Agilent Technologies, USA). Measurements were normalized by the sample total area.

Surface chemical composition was determined by X-ray photoelectron spectroscopy (XPS). A surface analysis system (SPECS, Germany) equipped with a Phoibos 150 electron analyzer was used for the measurements. The monochromatized Aluminum radiation (1486.6 eV) with the output power set at 380 W was used for the analyses of all samples. The C1s signal (284.6 eV) was employed as the reference to calibrate the binding energies (BE) of different elements in order to correct the charge effect. CasaXPS software was used to analyze all XPS data. Surface atomic concentrations in the samples were estimated using the instrument sensitivity factors to scale for the calculated photoelectron peak areas.

2.6. Bacterial adhesion assays

In order to test the antibacterial properties of nanofilms, *S. aureus* (ATCC 25933) and *P. aeruginosa* (ATCC 27853) bacteria cultures were performed in the laboratories of IPEL Itibanyl Products Special Ltda. Bacterial adhesion experiments were run in a biological safety cabinet (VLFS-12, Veco), in a positive pressure controlled room. Bacterial inocula at 1×10^6 CFU m/L were used for the experiments as initial concentration for culture in tryptic soy broth (TSB) medium. The samples were incubated in duplicate for 4 and 8 h in a bacterial incubator (model AP-22, Phoenix) at 36 °C without culture media replacement. Bacterial cell counting was performed by the dilution plating technique [5]. After specified bacteria culture times (4 or 8 h), the culture medium was removed to interrupt all growth; the samples were subsequently washed three times with deionized water to remove the constituents of the culture medium as well as non-attached cells and biofilms completely. Then, the samples were submitted to ultra-sonication in phosphate buffered saline solution (PBS) to remove the attached cells and they were consecutively diluted with PBS in (1:9 v/v) proportions. Aliquots of 0.2 mL of the obtained cell suspensions were then plated in triplicate onto solid agar medium using the spread plate method. After incubating for 24 h, the number of bacteria colonies was counted and the results, after multiplication by the dilution factor, were expressed as mean colony forming units (CFU) per cm^2. The average value was reported as mean ± SD of three measurements from triplicate cultures. Data were analyzed with Statgraphics Centurion XV software. The statistical difference was established using analysis of variance (ANOVA) multifactorial model; *p*-values of 0.05 or less were considered statistically significant.

3. Results and discussion

Si substrate preparation was evaluated by measuring the water contact angle after each step (Fig. S1). After plasma treatment, cleaned samples changed their wettability into a strong hydrophilic behavior, from 54° to 16°, due to the silanol groups formed by plasma oxidation [17,18]. In the same sense, after PEI deposition, samples changed their wettability into a more hydrophobic behavior, from 16° to 80°. This is because PEI is a highly positive charged polycation, which readily attaches to oxidized surfaces [19]. As PEI provides a more homogeneous electrical charge distribution onto the substrate surface [20], subsequent multilayer deposition is expected to be uniform as well.

We have calculated the ionization degree of each biopolymer for each pH value by means of the Henderson–Hasselbalch equation ($pH = pK_a + \log$(non-protonated species $[A^-]$/protonated species [HA])) [21] and the corresponding pK_a values of HA and CHI, 3 and 6.5, respectively [22]. HA and CHI were assembled by LbL at pH lower than 5 (4.5, 3 and 2) to keep CHI totally ionized since the ionized amino groups are strongly related to the antibacterial effect in HA/CHI nanofilms [10]. However, the HA ionization degree is very susceptible to acid pH values: at pH 4.5, HA is 100% ionized; at pH 3, HA is 50% ionized; and at pH 2, HA is just 9% ionized. Thus, a detailed physicochemical characterization is necessary to address the influence of these three considerably different degrees of HA ionization while holding CHI completely ionized.

HA and CHI assemblings were monitored by measuring their respective water contact angle and roughness in each outermost layer (Fig. 1A). Zig-zag profiles in the water contact angle measurements are formed because the respective functional groups of each biopolymer modulate the wettability behavior [10]; HA coatings with carboxylic groups are more hydrophilic than CHI coatings with amine groups. Our measurements show that the largest contact angles are observed for the films assembled at pH 4.5, while the smallest angles were shown by the films assembled at pH 2. According to previous works [5,23], highly charged polymer chains tend to be adsorbed as thin layers with flat chain conformations, while the less charged polymer chains adsorb as thicker, loopier-type structures. According to this model, a thin flat and ionized chain of HA at pH 4.5 would interact strongly with the previous hydrophobic PEI coating, reducing slightly the water angle contact from 80° to 58°. Contrarily, the thicker, loopier-type and less charged chain of HA at pH 2 would interact weakly with the PEI layer; in that case, HA would be more exposed on the surface, reducing significantly the water angle contact from 80° to 31°. An intermediate value for the case of HA layer at pH 3 is due to partial chain ionization.

Fig. 1A also shows the roughness of each outermost layer, and their corresponding 3D-AFM images are presented in Fig. S2. In the case of HA/CHI assemblies at pH 4.5 and 3, the root mean square roughness (R_{RMS}) increased as a function of the number of bilayers. Nevertheless, the sample synthetized at pH 2 presented a constant low R_{RMS} value (~1 nm). At pH 4.5 and 3, the polymer chains would be ionized and the consequent extended layers formed would then originate the corrugated coatings. Although both samples presented similar R_{RMS} values in the last layer, the mean grain size attained at pH 3 was higher than that at pH 4.5, around 190 and 120 nm, respectively (Fig. 1B). This can be explained due to the partial ionization of HA at pH 3, which prevents larger CHI integration into the nanofilms. This effect, in turn, generates grain swelling. In the case of pH 2, it is important to highlight the slight zig-zag observed in the R_{RMS} profile, with the higher (lower) R_{RMS} values for the HA (CHI) layers, respectively. This behavior suggests that the non-ionized, loopier-type structures of HA at pH 2 would form somewhat rough coatings, which would be smoothen out by the totally ionized and extended CHI chains. This effect is indeed observed in the AFM images as a function of the thickness, as shown in Fig. S2.

The morphology of the samples was also observed by FESEM (Fig. 1C). Samples obtained at pH 4.5 and 3 presented round features on the surface, which agree with AFM topography. The sample prepared at pH 2 showed a smoother surface with few small particles. This morphology also corresponded very well with its previous topography analysis by AFM.

In order to evaluate the sample thickness by AFM, we have removed a partial section of the nanofilm, forming a step between the Si substrate and the top CHI coating (Fig. S3). The thickness values thus obtained were 10 (±2), 20 (±5) and 15 (±3) nm for pH 4.5, pH 3 and pH 2, respectively, and were regulated by the ionization degree. In all three samples, pre-layer of PEI was very thin, with a thickness of 1.2 (±0.2) nm. At pH 4.5, both HA and CHI are totally ionized forming a very well integrated film. For pH 3 and pH 2, samples are thicker due to their lower ionization degree. This partial repulsion produces swelling of the films.

UV–vis spectroscopy of HA/CHI assemblies allowed us to measure free carboxylic and amino groups in our samples (Fig. 2A). Using oppositely charged stains, methylene blue (MB, positively charged) and rose Bengal (RB, negatively charged), free carboxylic groups of HA (negatively charged) and free ammonium groups of CHI (positively charged) were detected, respectively [10]. In the case of samples obtained at pH 4.5 and 3, clear zig-zag profiles are observed in the absorbance measurements. As expected, MB stain adsorption was more effective in HA than CHI layers (half vs integer number of bilayers, respectively). The opposite behavior was observed for the RB stain, with lower absorbance in HA than CHI layers. The pH 4.5 samples presented lower absorbance than pH 3, for both stains, because HA and CHI layers are very well integrated. As both biopolymers are totally ionized, free carboxylic and amine groups are not available to be attached with their respective stains. In the case of the pH 3 sample, a higher progressive accumulation of absorbance for both stains along the bilayers is observed.

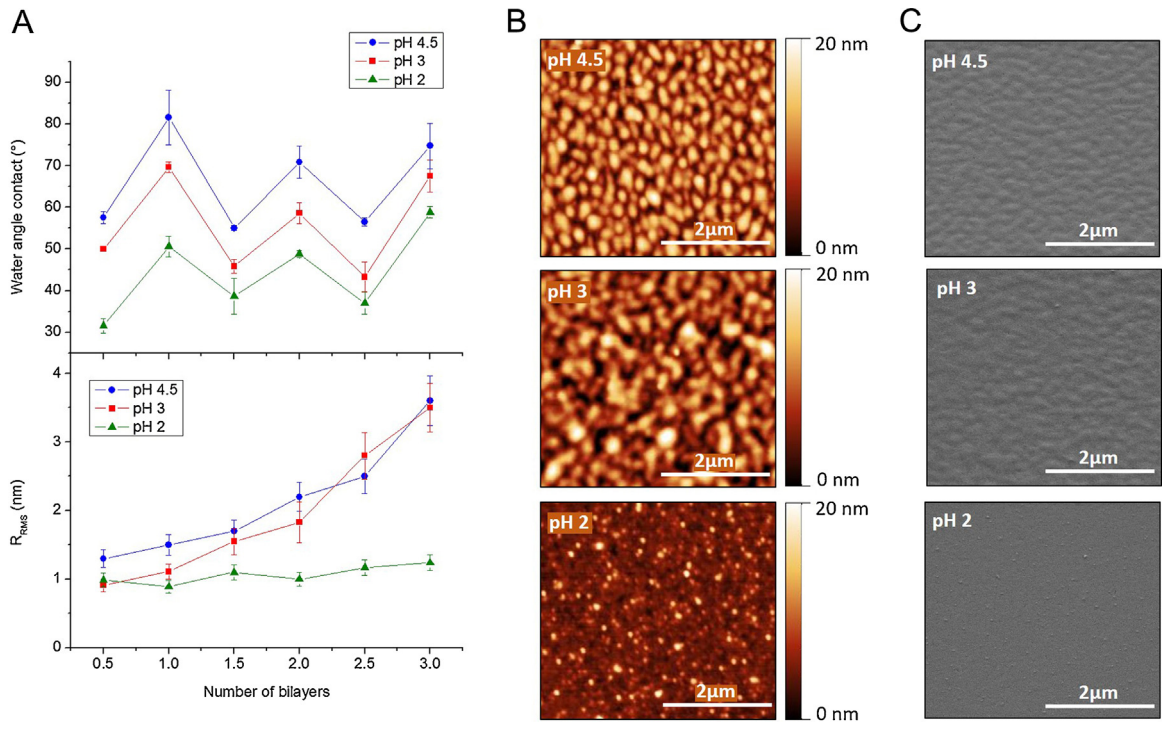

Fig. 1. (A) LbL monitoring of HA/CHI assembly by water contact angle technique and surface roughness measurements with AFM. Results represent mean ± SD of three measurements. (B) AFM topography images and (C) FESEM images of nanofilms.

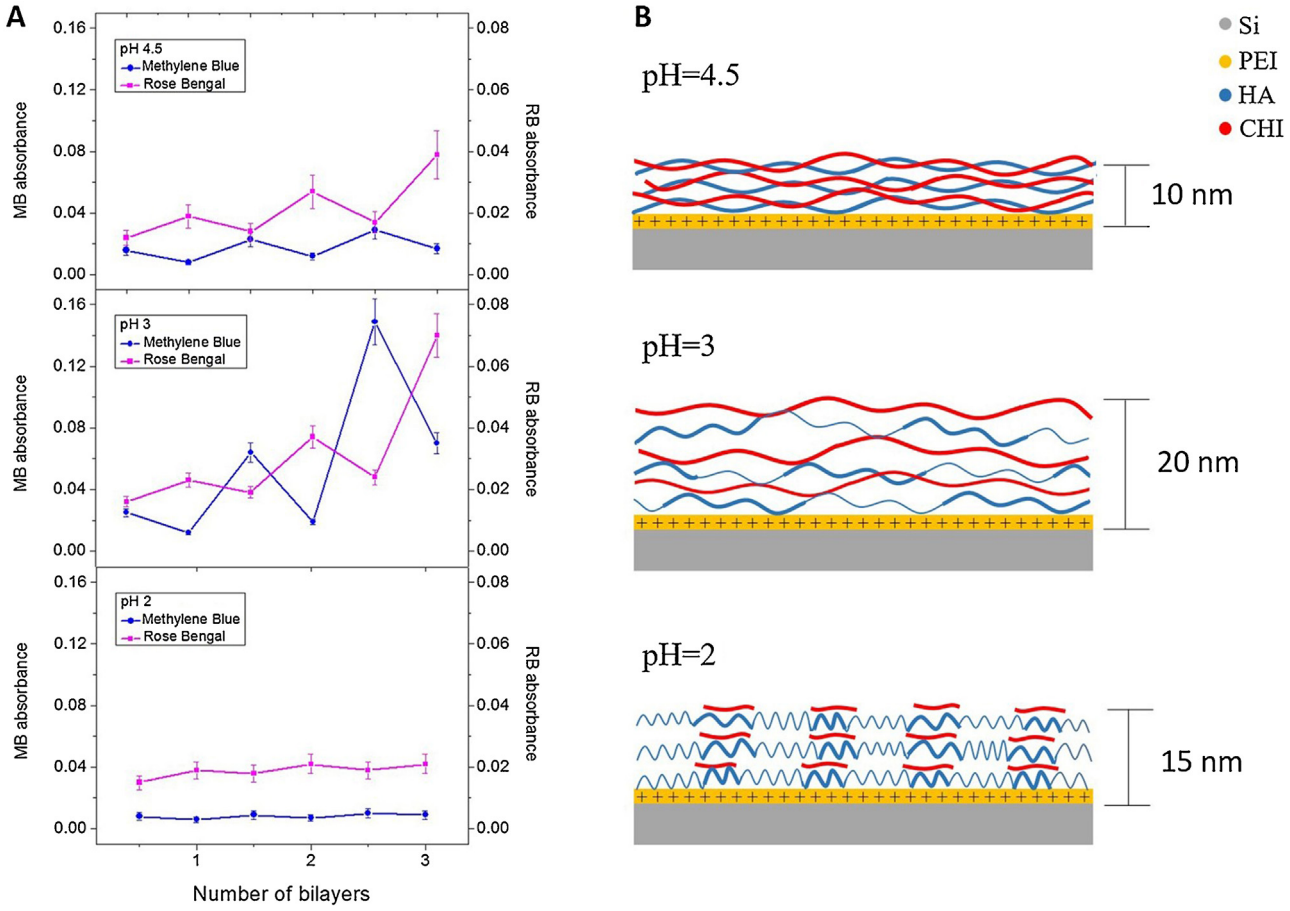

Fig. 2. (A) LbL monitoring of HA/CHI assembly by UV–vis spectroscopy. MB and RB are acronyms of methylene blue and rose Bengal stains, respectively. Results represent mean ± SD of three measurements. (B) A schematic model of the HA/CHI nanofilm formation as a function of the pH of assembly. Thick lines represent ionized biopolymer and thin lines represent unionized biopolymer.

This is explained by the partial ionization of HA, and the resulting lower attraction between HA and CHI layers, leaving more free ammonium groups available to the stain. However, the pH 2 sample did not follow the previous trend: at lower pH of assembly, stain absorbance is higher. This is probably due to the low ionization of HA layers of the pH 2 sample, which prevents a homogeneous attachment to the surface; subsequently, the unionized chains of HA would not be available to interact with CHI layers, even when CHI is totally ionized. Based on the previous surface physicochemical characterizations, a schematic model of the HA/CHI nanofilms formation as a function of the pH of assembly is presented in Fig. 2B.

The antibacterial effect of the obtained HA/CHI nanofilms was then tested with both types of bacteria, *S. aureus* and *P. aeruginosa* (Fig. 3). It seems very clear that the *S.aureus* bacteria were very sensitive to the surface of nanofilms assembled at different pH. Compared to the control sample (Si substrate), the pH 4.5 sample reduced bacterial density by 1 and 2 orders of magnitude of CFU/cm^2 at 4 and 8 h of cell culture, respectively. The antibacterial effect of the pH 3 sample was more impressive for both culture times, reducing cell density by 3 orders of magnitude for 4 h and 5 orders for 8 h. In the case of pH 2, no reduction of the bacterial density was observed for both culture times. This could be explained by the schematics in Fig. 2B. With the low CHI density at the sample top layer, the HA would be exposed, promoting cell adhesion [24]. The response of bacteria growth on our samples provides support to the hypothesis that free ammonium groups on the top CHI layer rule the antibacterial effect. However, in the case of *P. aeruginosa* cultures for 4 h, pH 4.5 and pH 3 samples did not show important antibacterial effect; bacteria have grown at slightly lower rates when compared to the Si substrate. Nevertheless, these samples could reduce the *P.aeruginosa* density by 1 order of magnitude of CFU/cm^2 at 8 h of culture. For the pH 2 sample, as the case of the *S. aureus* assay, the bacterial density was unaltered for both culture times.

Due to the encouraging results against *S. aureus*, the evolution of the surface chemistry of the pH 3 sample was studied by XPS. The C1s and N1s core level spectra of first HA layer, subsequent CHI layer (HA/CHI), and HA/CHI layer after three cycles ((HA/CHI)$_3$) are shown in Fig. 4A. The C1s envelope can be fitted with four components corresponding to C—C/CH (284.5 eV), C—O (286.0 eV), C═O/O—C—O (287.5 eV) and COO— (289.2 eV) [25], which are related to both biopolymers, HA and CHI [26]. Quantitative composition analyses, obtained from the relative intensities of the peaks, are shown in Table 1. The ionized carboxylic group (COO^-) relative intensity in the first HA layer (5.8%) is reduced to 3.6% due to CHI incorporation, and a further reduction to 1.6% in (HA/CHI)$_3$ due to the deposition of subsequent layers. In the N1s core level spectra, the chemical evolution of samples was also observed. The fitting curve analysis for the first HA layer presented a dominant composition of amine groups (NH_2), due to the PEI layer (Fig. S4A), and a low percentage of ammonium groups (NH_3^+). After CHI deposition, NH_3^+ increased from 10.5% to 43% (Table 1). The presence of NH_3^+ groups is also significantly higher in the (HA/CHI)$_3$ layer with 34%. Additionally, it is important to mention that, in the HA/CHI layer, the extra ═N— group detected is related to the crosslinking of CHI with PEI [27], which was not longer observed in the (HA/CHI)$_3$ layer. These results suggest that the presence of amine and ammonium groups exposed on the surface are the main cause for the antibacterial effect. In order to confirm these results, XPS analyses on the pH 4.5 sample was also performed; Fig. 4B shows the deconvolution of its N1s core level spectrum. The spectrum presented three components corresponding to NH_2 (399.1 eV), —NHCO (400.5 eV) and NH_3^+ (401.8 eV) [28]. The amine (NH_2) and ammonium (NH_3^+) peaks originate from CHI, and the amide (—NHCO) peak from HA [10]. This agrees with our schematic model (Fig. 2B): at pH 4.5, HA and CHI layers are very well integrated and both are exposed on the top of the film. Moreover, the quantitative composition analyses (Table 2) indicates a considerably lower percentage of amine and ammonium, due to the amide contribution. This explains the lower antibacterial effect of pH 4.5 when compared with pH 3, as well as confirms the impact of the NH_2/NH_3^+ surface composition for an enhanced antibacterial effect.

We can thus expect this effect to scale up with increasing density of amine and ammonium groups on the surface. In order to check this hypothesis for the pH 3 sample, we have increased the number of bilayers, from 3 to 9, since after several cycles of deposition, HA/CHI nanofilm thicknesses present an exponential growth trend (Fig. 5A). This behavior means that larger biopolymer mass values are incorporated in each layer along with the number of bilayers. This should also be valid for the density of free ammonium groups. Fig. 5B shows the absorbance values of adsorbed RB stain on coatings from the 1st to 3rd and from 7th to the 9th bilayer. However, as those values correspond to the absorbance accumulated along the HA/CHI depositions, the net values of RB absorbance for each bilayer are presented in Fig. 5C. Such net values were calculated by subtracting the absorbance value obtained in "n" bilayers from the absorbance measured in "n-1" bilayers. These results indicate that, for the 9th bilayer, the RB stain adsorption was 4 times larger than for the 3rd bilayer. If the growth trend of HA/CHI nanofilm thicknesses were linear, we would expect the net RB absorbance to be constant for each case. Therefore, the higher RB stain on the top of the 9-bilayer sample means a larger density of nitrogenated groups including free NH_3^+ than on the top of the 3-bilayer sample.

These results were confirmed by surface potential measurements on both samples. Fig. 5D and E show topography and surface potential images of steps between the Si substrate (dark areas) and nanofilms (light areas), respectively. The surface potential profile of the 9-bilayers sample shows twice the height of the 3-bilayers sample, approximately 150 and 75 mV, respectively (Fig. 5F). As the surface potentials of nanofilms are assumed to be mainly generated by NH_3^+ of the top CHI layer [10], this result agrees very well to those obtained by UV–vis spectroscopy.

The antibacterial effect of the 9-bilayers sample was also tested with *S. aureus* and *P. aeruginosa* strains (Fig. 6). In the case of *S. aureus* assay, bacteria were not detected in any of the culture times, confirming the enhanced effectivity of the ammonium groups of HA/CHI nanofilms as a biocide agent for *S. aureus*. A similar approach was taken by Richert et al. [15]. These authors increased the salt concentration from 10^{-2} to 0.15 M NaCl for their HA/CHI assembling at pH 5, obtaining films with thickness values of 120 and 300 nm, respectively. In their case, the thicker films presented better antimicrobial effect (against *E. coli*), similarly to our results. However, those authors attribute the enhanced antibacterial behavior to a larger rigidity, despite the lack of any mechanical properties characterization. Our results suggest that the larger amount of free ammonium groups on the top CHI layer of the thicker nanofilm is the most important parameter for the antibacterial effect against *S. aureus*.

In the case of *P. aeruginosa*, the larger amount of nitrogenated groups on the top film of the thicker sample did not provide a significant change in the antibacterial effect. The 9-bilayers sample presented the same antibacterial effect as the 3-bilayers sample: a reduction of 1 order of magnitude of CFU/cm^2 for 8 h of culture. The enhanced resistance of the gram-negative *P. aeruginosa* against our nanofilms can be explained by the outer cell membrane [29], which protects the cell wall from the biocide contact of free ammonium groups. Although other gram-negative bacteria, such as *E. coli*, have been eliminated by CHI films [5], *P. aeruginosa* is usually more robust, forming larger biofilms than *E. coli* [30].

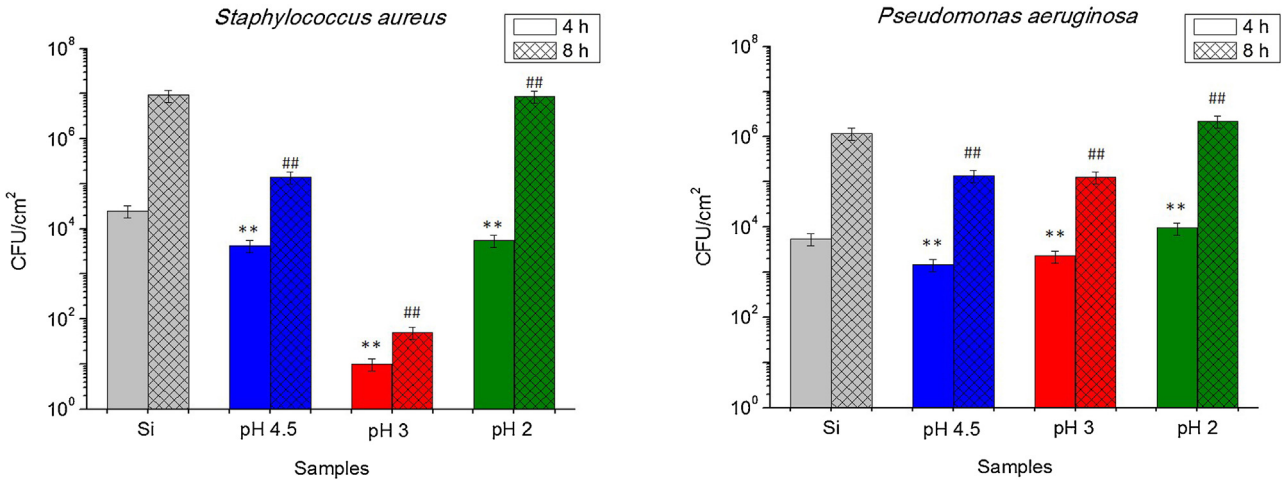

Fig. 3. Antibacterial effect of HA/CHI nanofilms. The number of viable bacteria on the samples at 4 and 8 h was determined using the spread plate method. Results represent mean ± SD of three measurements, statistically interpreted by analysis of variance (ANOVA) multifactorial model. ** denotes a significant difference compared to the Si substrate at 4 h ($p < 0.01$); -denotes a significant difference compared to the Si substrate at 8 h ($p < 0.01$).

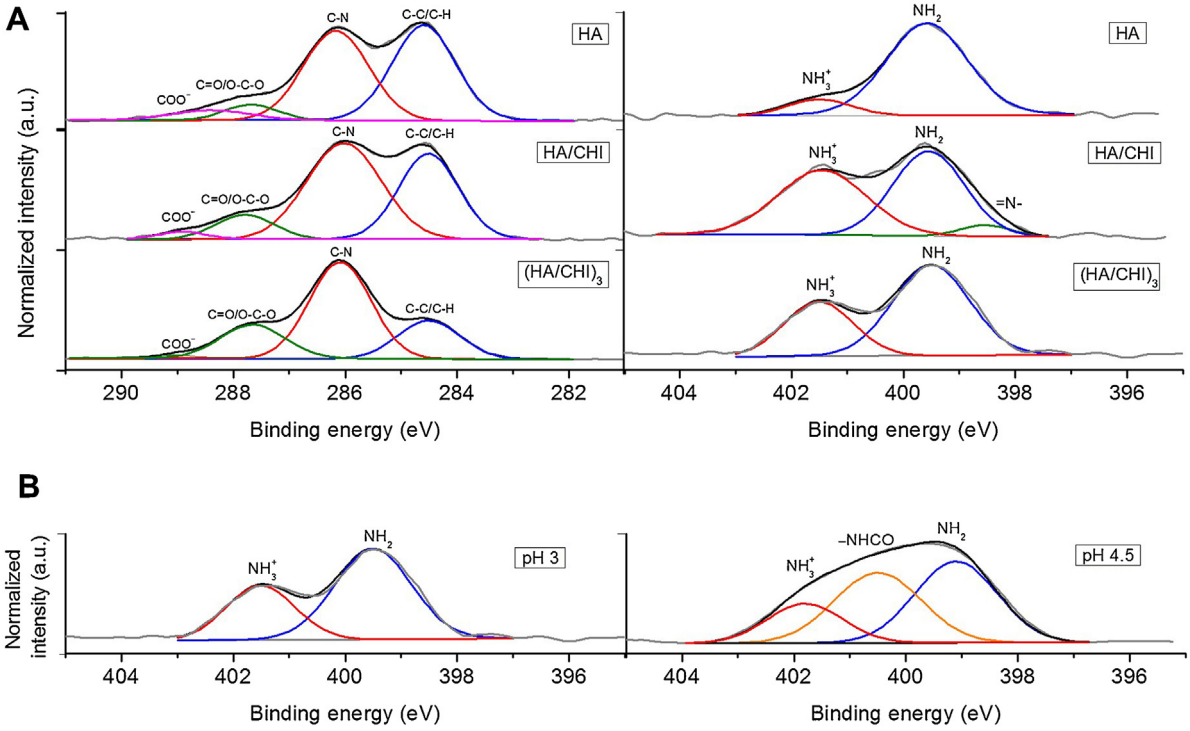

Fig. 4. (A) Evolution of the surface chemistry of the pH 3 sample by XPS. C1s and N1s core level spectra of HA, HA/CHI and $(HA/CHI)_3$. (B) N1s core level spectra of the pH 3 and pH 4.5 samples.

Table 1
XPS results of C1s and N1s fitting curve for HA, (HA/CHI) and $(HA/CHI)_3$ samples obtained at pH 3. Results represent mean ± SD of three fittings.

C 1s corresponding groups	HA		HA/CHI		$(HA/CHI)_3$	
	Peak	%	Peak	%	Peak	%
C—C/C—H	284.5	45.3 (±0.4)	284.6	42.5 (±0.4)	284.5	22.1 (±0.2)
C—O	286.0	43.0 (±0.4)	286.1	42.2 (±0.4)	286.1	55.2 (±0.5)
C=O/O—C—O	287.8	5.9 (±0.1)	287.7	11.6 (±0.1)	287.7	21.0 (±0.2)
COO—	288.9	5.8 (±0.1)	288.4	3.6 (±0.1)	289.0	1.6 (±0.1)
N 1s corresponding groups	HA		HA/CHI		$(HA/CHI)_3$	
	Peak	%	Peak	%	Peak	%
=N—	–	–	398.5	4.5 (±0.1)	–	–
NH_2	399.6	89.5 (±0.9)	399.5	45.3 (±0.4)	399.5	66.0 (±0.7)
NH_3^+	401.5	10.5 (±0.1)	401.5	43.0 (±0.4)	401.6	34.0 (±0.3)

Table 2
XPS results of N1s fitting curve for samples obtained at pH 3 and 4.5 after three cycles. Results represent mean ± SD of three fittings.

N 1scorresponding groups	pH 3		pH 4.5	
	Peak	%	Peak	%
NH_2	399.5	66.0 (±0.7)	399.1	43.0 (±0.4)
–NHCO	–	–	400.5	39.1 (±0.4)
NH_3^+	401.6	34.0 (±0.3)	401.8	17.9 (±0.2)

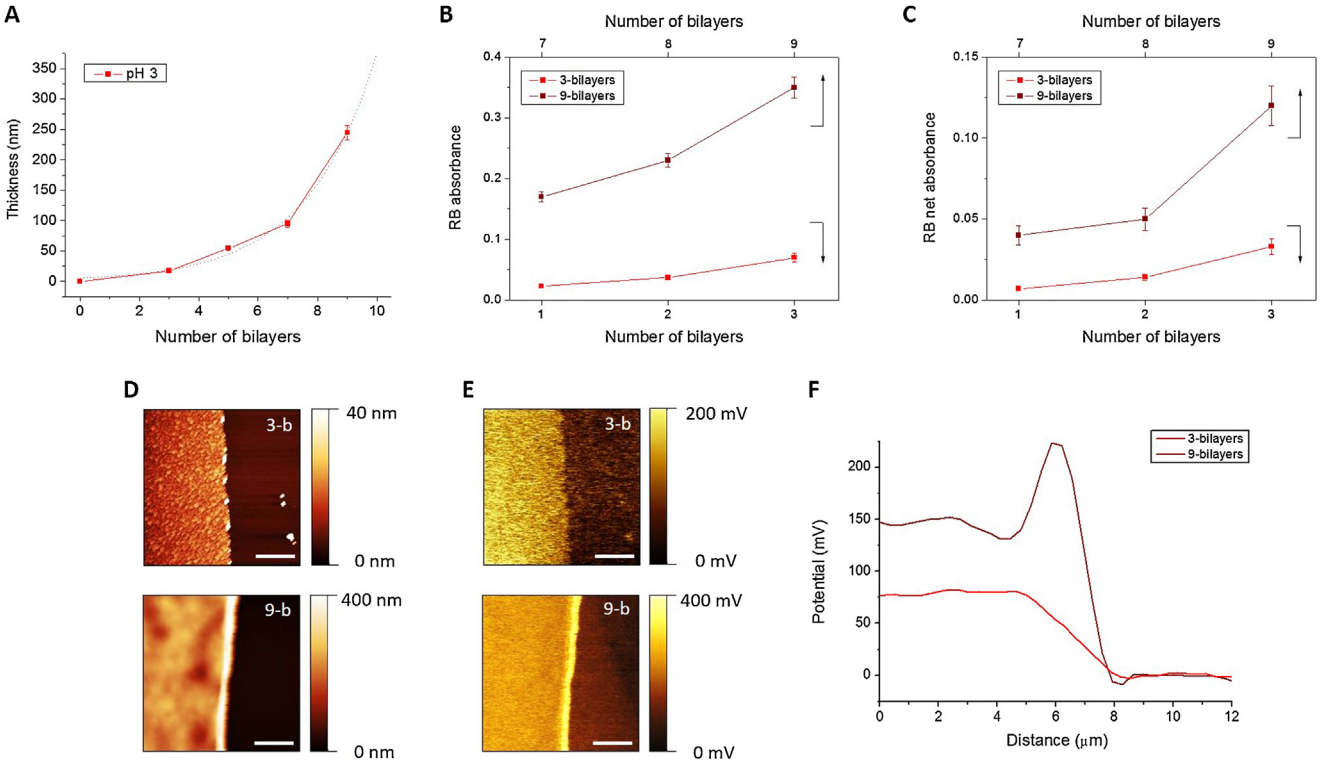

Fig. 5. (A) Thickness profile of the pH 3 sample (dotted line shows the exponential fitting). (B) LbL monitoring of the 6th to 9th bilayer assembly of the pH 3 sample by UV–vis spectroscopy. (C) RB net absorbance of top bilayers of the pH 3 samples. MB and RB are acronyms of methylene blue and rose Bengal stains, respectively. For figures A, B and C, results represent mean ± SD of three measurements. (D) Topography and (E) Surface potential images of nanofilm/Si substrate step (scale bar: 5 μm). (F) Surface potential profiles.

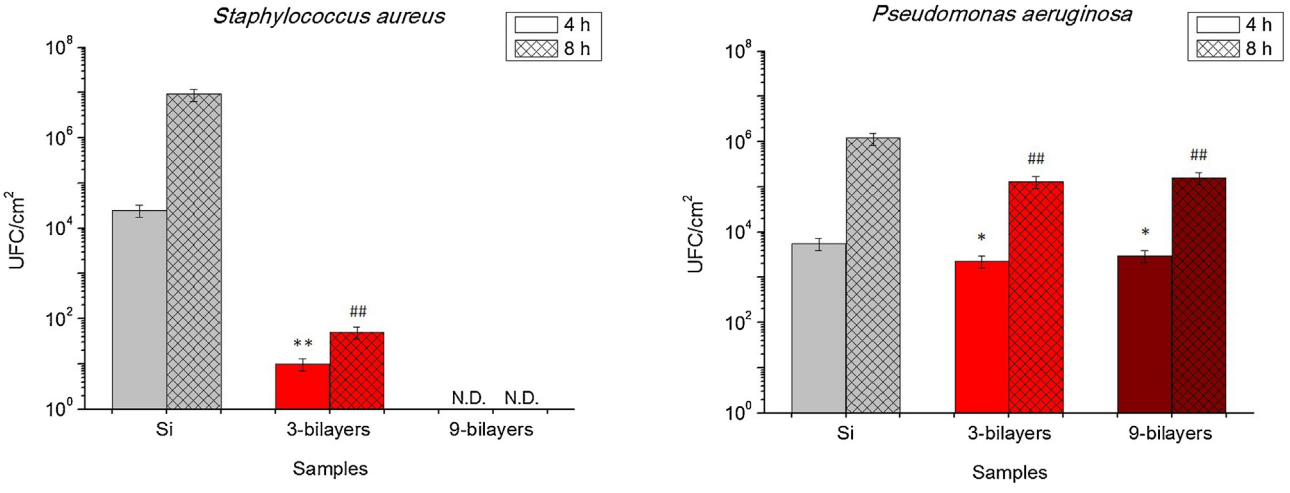

Fig. 6. Antibacterial effect of the pH 3 samples with 3-bilayers and 9-bilayers evaluated by the number of viable bacteria on the samples at 4 and 8 h as determined using the spread plate method. Results represent mean ± SD of three measurements, statistically interpreted by analysis of variance (ANOVA) multifactorial model. * and ** denote a significant difference compared to the Si substrate at 4 h with $p < 0.05$ and $p < 0.01$, respectively; -denotes a significant difference compared to the Si substrate at 8 h ($p < 0.01$). N.D. means not detected.

4. Conclusions

HA/CHI nanofilms assembled by LbL technique with different pH values of the biopolymer stem-solutions, which control their ionization degree, were studied in detail as antibacterial coatings. Due to the important impact in medicine, as mains precursors of nosocomial infections, *S. aureus* and *P. aeruginosa* were used to test the nanofilms as antibacterial surfaces. We observe a good correlation between the nanofilm surface physicochemical properties and the obtained antibacterial effect; we have thus explored the exponential growth trend of nanofilm thickness to maximize this effect on thicker samples. In the case of *S. aureus*, the bacterial growth was very sensitive to the free ammonium groups on the top CHI layer of our samples. In that sense, the antibacterial effect of the pH 3 sample was very relevant up to 8 h of culture, with total suppression of bacterial growth. For the *P. aeruginosa* assay, however, a slight antibacterial effect was observed for the 8 h of culture time, and bacterial growth rates at 4 h of culture were similar to those over the uncoated Si surface used as control. In conclusion, HA/CHI nanofilms in the optimized conditions of synthesis shown here are an excellent alternative as antibacterial surfaces against *S. aureus*. In particular, the resistance against *S. aureus* adhesion and proliferation for 8 h suggests that this coating should be suitable for prosthesis protection against contamination during surgery, for example. Nevertheless, their use against *P. aeruginosa* would require the addition of antimicrobial active species, such as bioactive peptides, silver nanoparticles and other suitable biocides.

Acknowledgements

We would like to thank Analytical Resources and Calibration Laboratory (LRAC) from Faculty of Chemical Engineering and Multiuser Lab (LAMULT) from Institute of Physics “Gleb Wataghin”, both from UNICAMP, for providing the analytical facilities. We would also like to thank the National Nanotechnology Laboratory (LNNano) for granting access to the electron microscopy facilities. This work was financially supported by FAPESP (grant numbers 2010/51748-7 and 2013/02300-1), CNPq and CAPES. J. Hernandez-Montelongo and V. Nascimento acknowledge FAPESP and FAPEAM scholarships, respectively.

Appendix A. Supplementary data

Supplementary data associated with this article can be found, in the online version, at http://dx.doi.org/10.1016/j.colsurfb.2016.02.028.

References

[1] W. Bereket, K. Hemalatha, B. Getenet, T. Wondwossen, A. Solomon, A. Zeynudin, et al., Update on bacterial nosocomial infections, Eur. Rev. Med. Pharmacol. Sci. 16 (8) (2012) 1039–1044.
[2] M.P. Deege, D.L. Paterson, Reducing the development of antibiotic resistance in critical care units, Curr. Pharm. Biotechnol. 12 (12) (2011) 2062–2069.
[3] T.J. Foster, J.A. Geoghegan, V.K. Ganesh, M. Höök, Adhesion, invasion and evasion: the many functions of the surface proteins of *Staphylococcus aureus*, Nat. Rev. Microbiol. 12 (1) (2014) 49–62.
[4] H. Loveday, J. Wilson, K. Kerr, R. Pitchers, J. Walker, J. Browne, Association between healthcare water systems and *Pseudomonas aeruginosa* infections: a rapid systematic review, J. Hosp. Infect. 86 (1) (2014) 7–15.
[5] J. Fu, J. Ji, W. Yuan, J. Shen, Construction of anti-adhesive and antibacterial multilayer films via layer-by-layer assembly of heparin and chitosan, Biomaterials 26 (33) (2005) 6684–6692.
[6] F. Croisier, C. Jérôme, Chitosan-based biomaterials for tissue engineering, Eur. Polym. J. 49 (4) (2013) 780–792.
[7] M. Benhabiles, R. Salah, H. Lounici, N. Drouiche, M. Goosen, N. Mameri, Antibacterial activity of chitin, chitosan and its oligomers prepared from shrimp shell waste, Food Hydrocolloids 29 (1) (2012) 48–56.
[8] M. Joshi, R. Khanna, R. Shekhar, K. Jha, Chitosan nanocoating on cotton textile substrate using layer-by-layer self-assembly technique, J. Appl. Polym. Sci. 119 (5) (2011) 2793–2799.
[9] B. Zhou, Y. Hu, J. Li, B. Li, Chitosan/phosvitin antibacterial films fabricated via layer-by-layer deposition, Int. J. Biol. Macromol. 64 (2014) 402–408.
[10] J. Hernández-Montelongo, V.F. Nascimento, D. Murillo, T.B. Taketa, P. Sahoo, A.A. de Souza, et al., Nanofilms of hyaluronan/chitosan assembled layer-by-layer: an antibacterial surface for *Xylella fastidiosa*, Carbohydr. Polym. 136 (2016) (2015) 1–11.
[11] P. Chua, K. Neoh, E. Kang, W. Wang, Surface functionalization of titanium with hyaluronic acid/chitosan polyelectrolyte multilayers and RGD for promoting osteoblast functions and inhibiting bacterial adhesion, Biomaterials 29 (10) (2008) 1412–1421.
[12] G. Cado, R. Aslam, L. Séon, T. Garnier, R. Fabre, A. Parat, et al., Self-defensive biomaterial coating against bacteria and yeasts: polysaccharide multilayer film with embedded antimicrobial peptide, Adv. Funct. Mater. 23 (38) (2013) 4801–4809.
[13] J. Fu, J. Ji, D. Fan, J. Shen, Construction of antibacterial multilayer films containing nanosilver via layer-by-layer assembly of heparin and chitosan-silver ions complex, J. Biomed. Mater. Res. A 79 (3) (2006) 665–674.
[14] J.J. Richardson, M. Björnmalm, F. Caruso, Technology-driven layer-by-layer assembly of nanofilms, Science 348 (6233) (2015) aaa2491.
[15] L. Richert, P. Lavalle, E. Payan, X.Z. Shu, G.D. Prestwich, J. Stoltz, et al., Layer by layer buildup of polysaccharide films: physical chemistry and cellular adhesion aspects, Langmuir 20 (2) (2004) 448–458.
[16] D. Cui, A. Szarpak, I. Pignot-Paintrand, A. Varrot, T. Boudou, C. Detrembleur, et al., Contact-killing polyelectrolyte microcapsules based on chitosan derivatives, Adv. Funct. Mater. 20 (19) (2010) 3303–3312.
[17] T. Suni, K. Henttinen, I. Suni, J. Mäkinen, Effects of plasma activation on hydrophilic bonding of Si and SiO2, J. Electrochem. Soc. 149 (6) (2002) G348–51.
[18] N. Naveas, V.T. Costa, D. Gallach, J. Hernandez-Montelongo, R.J.M. Palma, J.P. Garcia-Ruiz, et al., Chemical stabilization of porous silicon for enhanced biofunctionalization with immunoglobulin, Sci. Technol. Adv. Mater. 13 (4) (2012) 045009.
[19] W. He, R.V. Bellamkonda, Nanoscale neuro-integrative coatings for neural implants, Biomaterials 26 (16) (2005) 2983–2990.
[20] T.D. Martins, R.A. Bataglioli, T.B. Taketa, F. da Cruz Vasconcellos, M.M. Beppu, Surface modification of polyelectrolyte multilayers by high Radio frequency air plasma treatment, Appl. Surf. Sci. 329 (2015) 287–291.
[21] E. Pâslaru, L. Fras Zemljic, M. Bračič, A. Vesel, I. Petrinić, C. Vasile, Stability of a chitosan layer deposited onto a polyethylene surface, J. Appl. Polym. Sci. 130 (4) (2013) 2444–2457.
[22] C. Vasile, D. Pieptu, R.P. Dumitriu, A. Panzariu, L. Profire, Chitosan/hyaluronic acid polyelectrolyte complex hydrogels in the management of burn wounds, Rev. Med. Chir. Soc. Med. Nat. Iasi. 117 (April–June (2)) (2013) 565–571.
[23] D. Yoo, S.S. Shiratori, M.F. Rubner, Controlling bilayer composition and surface wettability of sequentially adsorbed multilayers of weak polyelectrolytes, Macromolecules 31 (13) (1998) 4309–4318.
[24] F.C. Vasconcellos, A.J. Swiston, M.M. Beppu, R.E. Cohen, M.F. Rubner, Bioactive polyelectrolyte multilayers: hyaluronic acid mediated B lymphocyte adhesion, Biomacromolecules 11 (9) (2010) 2407–2414.
[25] J. Hernandez-Montelongo, N. Naveas, S. Degoutin, N. Tabary, F. Chai, V. Spampinato, et al., Porous silicon-cyclodextrin based polymer composites for drug delivery applications, Carbohydr. Polym. 110 (2014) 238–252.
[26] J. Almodóvar, L.W. Place, J. Gogolski, K. Erickson, M.J. Kipper, Layer-by-layer assembly of polysaccharide-based polyelectrolyte multilayers: a spectroscopic study of hydrophilicity, composition, and ion pairing, Biomacromolecules 12 (7) (2011) 2755–2765.
[27] S.W. Won, I.S. Kwak, Y. Yun, The role of biomass in polyethylenimine-coated chitosan/bacterial biomass composite biosorbent fiber for removal of Ru from acetic acid waste solution, Bioresour. Technol. 160 (2014) 93–97.
[28] G. Lawrie, I. Keen, B. Drew, A. Chandler-Temple, L. Rintoul, P. Fredericks, et al., Interactions between alginate and chitosan biopolymers characterized using FTIR and XPS, Biomacromolecules 8 (8) (2007) 2533–2541.
[29] T.R. De Kievit, R. Gillis, S. Marx, C. Brown, B.H. Iglewski, Quorum-sensing genes in *Pseudomonas aeruginosa* biofilms: their role and expression patterns, Appl. Environ. Microbiol. 67 (April (4)) (2001) 1865–1873.
[30] A. Culotti, A.I. Packman, *Pseudomonas aeruginosa* promotes escherichia coli biofilm formation in nutrient-limited medium, PLoS One 9 (9) (2014) e107186.